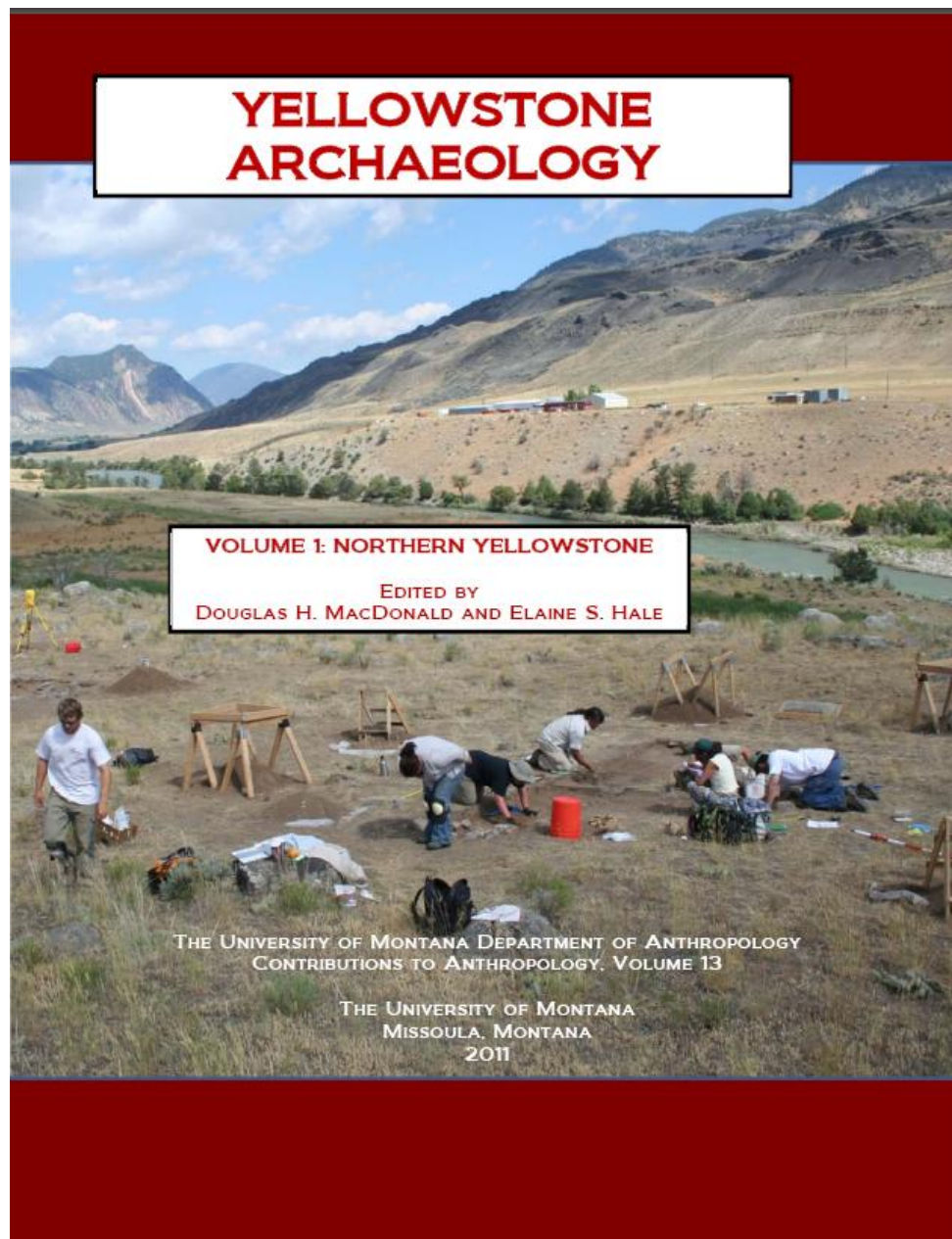


Total Field Magnetic Experiments at a Historic Town Site, Yellowstone National Park, USA: Aeromagnetic Techniques and Archaeological Targets

**By: Steven D. Sheriff
Department of Geosciences
University of Montana
Missoula
Montana USA**

in Yellowstone Archaeology, Volume 1: Northern Yellowstone; p. 26-40. Edited by D. H. MacDonald and E. S. Hale; The University of Montana Department of Anthropology Contributions to Archaeology, Volume 13, 143 p.



Introduction

The Montana-Yellowstone Archaeological Project, a joint endeavor of The University of Montana Department of Anthropology and Yellowstone National Park, studies the prehistory and history of the northern portion of Yellowstone National Park (MacDonald, 2007). The historical component of interest entails identifying the former location and extent of Cinnabar (figure 1), the original Northern Pacific Railroad depot for visitors to Yellowstone National Park between 1883 and 1903.

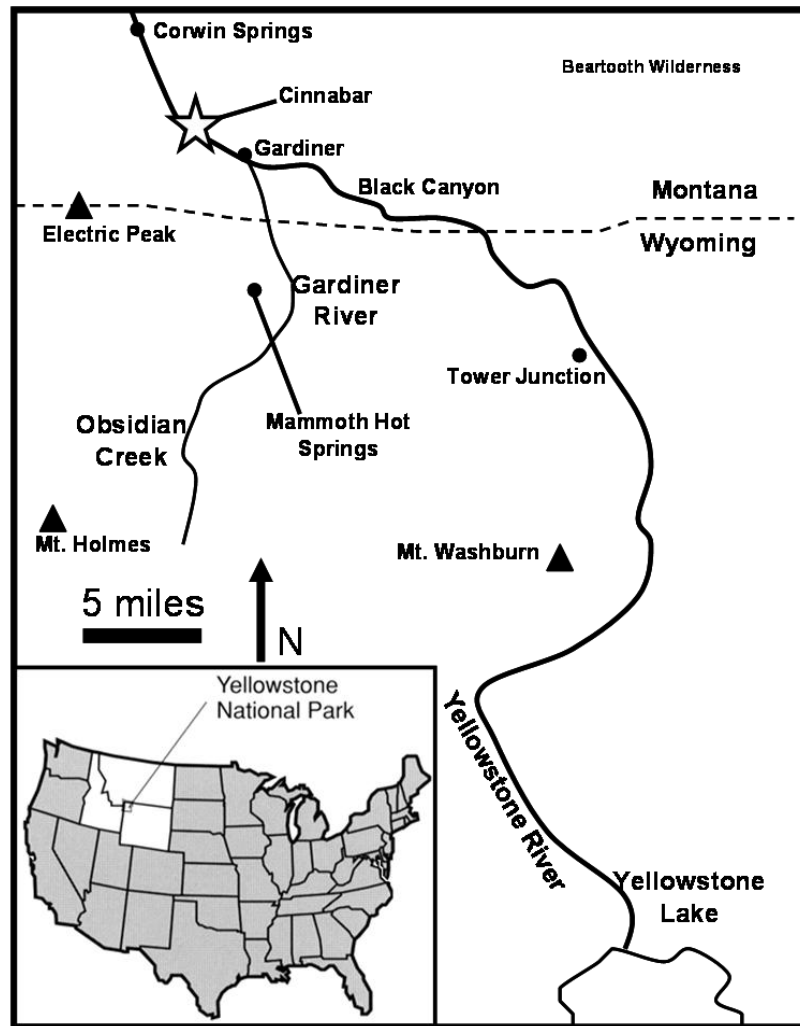


Figure 1. Index map locating the historic town of Cinnabar near Yellowstone National Park, Montana, USA.

The main area of Cinnabar contains the remains of 11 building foundations, identifiable as depressions upon the current ground surface. Yet a modern layer of up to 10 cm of silty aeolian sand complicates recognition of the vestiges of old structures in much of the area.

Individuals traveling to Yellowstone on the railroad photographed the central areas of Cinnabar during the late-19th century. Limited oral history along with two old photographs provides some guidance to the limits of Cinnabar. The historic photographs also helped corroborate archaeological field efforts within specific building foundations, such as the hotel, store, privy, and blacksmith shop. The area southeast of central Cinnabar (figure 2) lacks building foundations,

any adequate photography, or any surface-indication of former buildings. However, the area contains a scatter of historical debris, a possible indicator of buried archaeological deposits associated with Cinnabar. We chose to assess a portion of the area with total field magnetic observations in order to delineate buried or otherwise obscured features from the outlying parts of Cinnabar. Such exploration yields guidance for subsequent archaeological test units.

Archaeological geophysicists commonly choose to use magnetic gradiometry over total field magnetics at both historic and prehistoric sites (e.g. Aspinall, Gaffney, and Schmidt, 2008). Measuring total field intensity is often a better choice because measuring the gradient of the magnetic field accentuates the signal from debris lying on or near the surface (where visual detection is more efficient) at the expense of subtle signals from buried features. Magnetic gradiometry also requires closer sample intervals due to the more rapid decrease of anomalies with distance than that for total field intensity. Consequently, acquisition of total field intensity observations can speed field time.

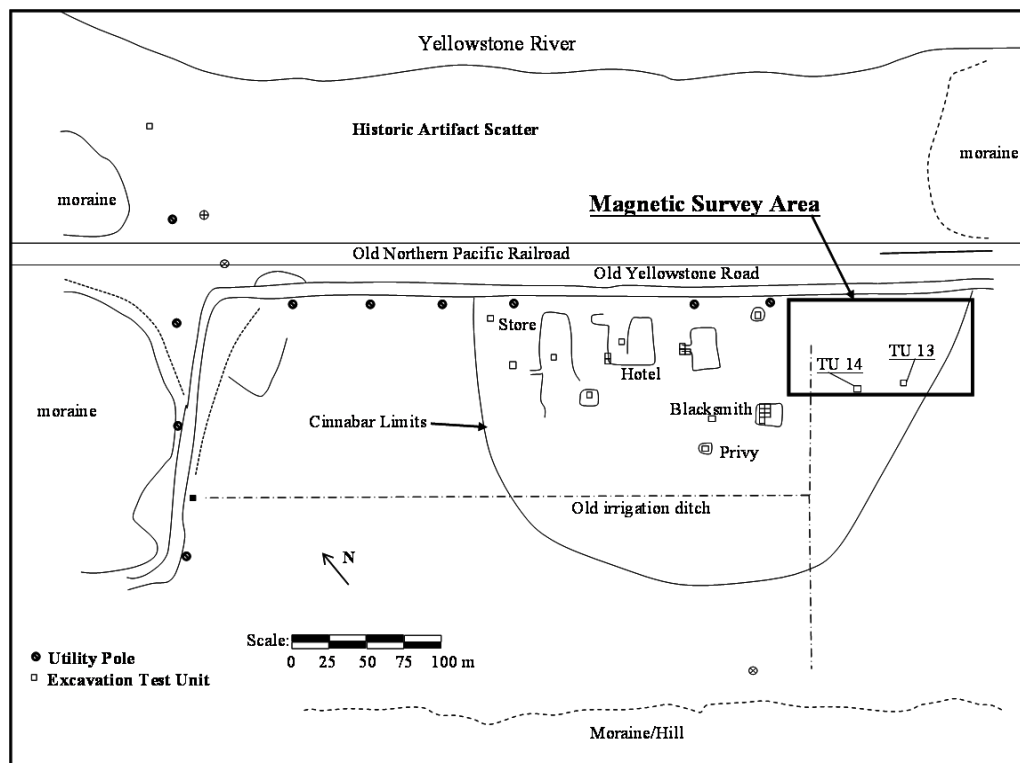


Figure 2. Site plan map for the archaeological study at Cinnabar.

At historic archaeological sites in the western United States, scattered ferromagnetic debris seems ubiquitous. This randomly scattered debris complicates magnetic surveys and interpretation at historic town sites (e.g. Kvamme, 1998; Larson et al., 1999), particular mining towns, in the western United States. Such debris may include steel cans, lumber, horseshoes, nails, roofing steel, machinery parts, and other cultural artifacts such as flower containers in cemeteries. In archaeological work at such sites we typically seek signals from residential foundations, building perimeters, or perhaps corral and stable boundaries. Those features of interest usually have a length scale of meters to several meters or more. The lower part of that spatial range is also the upper range of magnetic anomalies from the surface litter. We locate and map that debris when it

lies on the surface. Unfortunately the magnetic signal of ferromagnetic surface scatter, with its steep gradients and high amplitudes, dominates contour scales and obscures more subtle anomalies having longer spatial wavelengths. Often we wish to separate the signals from sources at varying depths with different spatial dimensions.

Separating the longer wavelength anomalies from deeper sources with respect to shallow sources requires collecting observations of total field magnetic intensity as opposed to magnetic gradiometry. Separation filtering of potential fields is a classic topic including techniques in the Fourier domain (e.g. Syberg, 1972; Jacobsen, 1987) or using wavelet transforms (e.g. Fedi and Florio, 2003; Paoletti et al., 2007). The filtering we find most appropriate and successful for separating sources on or near the ground surface from those buried in the shallow subsurface is matched filtering (Syberg, 1972; Phillips, 2001). Matched bandpass filtering entails fitting the radially averaged power spectrum of the total field magnetic data with a series of power spectra corresponding to simple equivalent layers at the archaeological site. For data with little impact from surface debris upward continuation by an amount equal to one half the line spacing works well.

Beyond matched filtering and upward continuation, we successfully treated our total field data to other processing techniques standard in aeromagnetic and ground magnetic exploration for mineral and energy resources using readily available software. These techniques include decorrugation (Urquhart, 1988), the pseudogravity transform Baranov (1957), and calculation of the horizontal and total gradients for edge detection. Though not commonly used in archaeological applications, we exploit these methods not only for experimentation but because they offer a number of advantages for filtering noisy data, separating sources, edge detection, and preparation for existing visualization and inversion packages (e.g. MAG3D, 2007).

Excavation of test units following the magnetic survey and our processing clearly indicate the remains of a buried domestic feature, perhaps the foundation to a house or other building, associated with the late-19th to early-20th century use of Cinnabar. The application of matched filtering to another test plot demonstrates its ability to filter the effects of scattered surface debris. Thus, application of these processing techniques in areas of archaeological interest with difficult acquisition situations or substantial surface scatter is worthwhile.

Magnetic Survey

We acquired total field magnetic intensity observations (figure 3) at 5 Hz while walking bidirectional transects spaced one meter apart using a Geometrics G858 Cesium vapor magnetometer. We used ropes and tape measures for spatial guidance during acquisition. Walking marked lines typically adds noise to the desired signal due to mislocations, sensor movement, variable walking speeds, and directionally dependent sampling frequencies; rugged surface conditions add additional noise during acquisition. We countered these problems with post-acquisition filtering, experimenting with several filtering techniques developed for aeromagnetic scale surveys designed to delineate tectonic features or for exploration by the energy and mining industries.

We collected our total magnetic field intensity data in about three hours on a magnetically quiet day as observed by NOAA (NOAA, 2009) and our on-site observations. There was neither forecast nor observed sunspot activity sufficient to drive significant magnetic variations during the

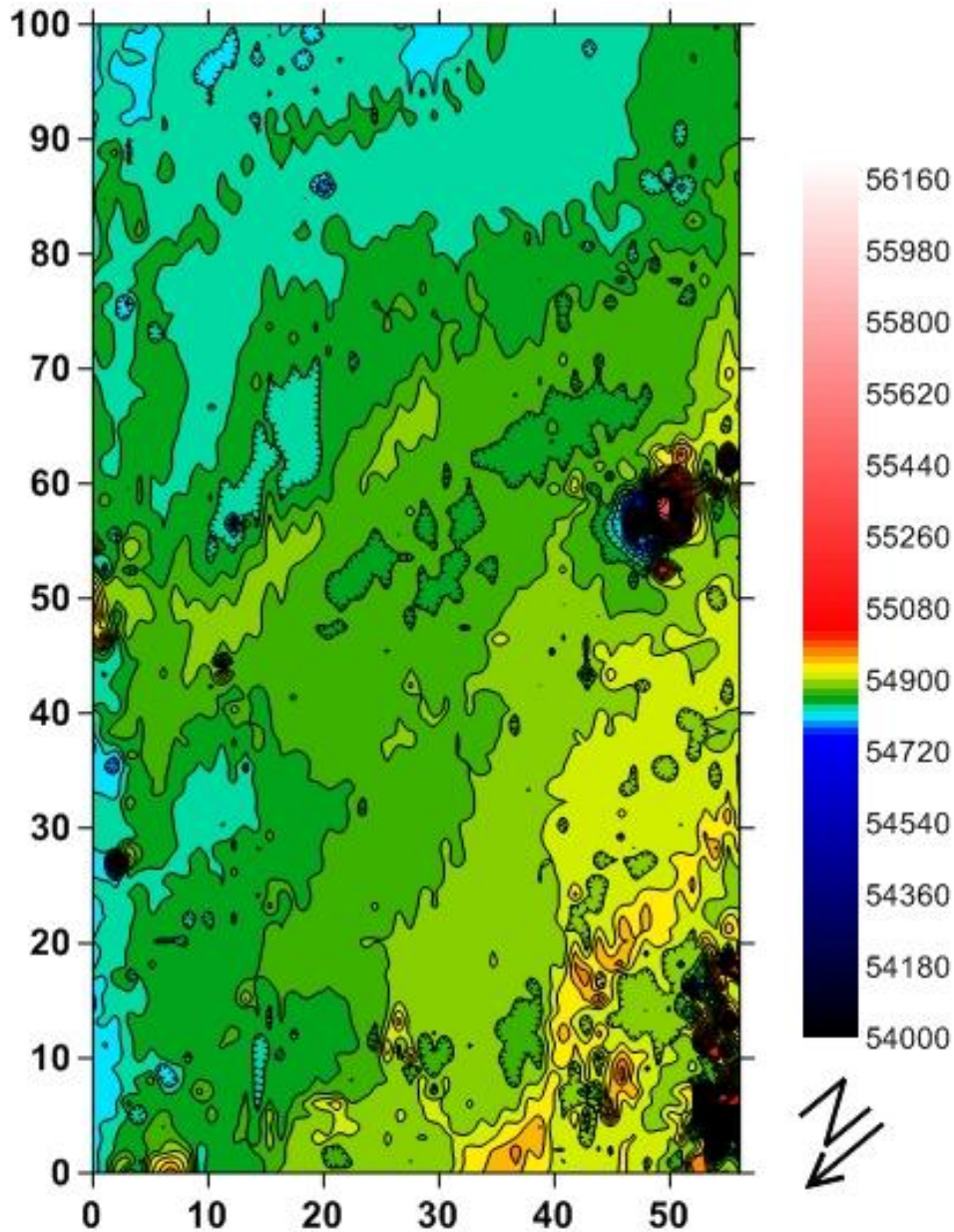


Figure 3. Total field intensity contoured at 10 nanotesla (nT); horizontal dimensions are meters. The vertical axis trends 130° east of north. The bidirectional acquisition direction, with one meter spacing, is vertical in the figure. The corrugation is apparent as the periodic herringbone pattern on north-south contours.

time in which we completed our survey. In confirmation, successive and repeat observations at stationary sites during the day showed minimal high frequency variance of the total magnetic field. Regardless, given our lack of a recording base station, geomagnetic variations will be present in the data. The frequency spectrum of such geomagnetic variance can be broad. Low frequency components have periods similar to the acquisition time of several transects and longer. High frequency components have periods ranging from the time for acquiring a few observations

to that for acquiring a few transects. In the filtering described below, we deal with the possibility of long period geomagnetic variation in combination with that for regional, or geologic, sources. We treat the potential effects of high frequency variance with filtering techniques adapted from the energy and mining industry. This proved successful as is demonstrated by the final maps. The ultimate anomalies of interest in this project have amplitudes of 10's to 100's of nanoteslas.

Our total magnetic field intensity observations (figure 3), gridded by kriging, include features at several scales. First, there is corrugation (also referred to as striping, zigzag, herringbone, or staggering) which is typical in ground and airborne magnetic surveys where observations are acquired at relatively high spatial frequency along more widely spaced transects. Despite the usual efforts to keep the sensor a constant distance from the ground, bunch grass, rough surfaces, rocks and wind combine to interfere with the operator and impact the distance of the sensor from the ground while walking and acquiring observations at 5 Hz. This manifests as linear magnetic anomalies highly correlated with the direction of acquisition. There are several methods for decorrugating magnetic data.

Urquhart (1988) developed a widely used technique for decorrugation filtering of aeromagnetic data. We use this, as discussed below, because it operates rapidly on a grid of data, allows visual inspection of results from successively larger filter operators, and thus empirical determination of a suitable operator size. Urquhart's (1988) method is also readily available in public domain software (Phillips, 1997, 2007). Other methods are more common among archaeological geophysicists who have generally performed line by line adjustments as opposed to filtering a complete grid of data. For example Ciminale and Loddo (2001) align nearest neighbor traces using correlation, Becker (2001) uses a GPS based speed dependent correction, and Odah et al. (2005) translate every other line by up to 1.5 meters to clean their data. Those choices have been in part dependent on available equipment and accompanying software. More recent contributions from Tsivouraki and Tsokas (2007) and Fedi and Florio (2003) address denoising and corrugation respectively and provide alternative methods for grid filtering based on the discrete wavelet transform. Regardless of the algorithm, decorrugating a magnetic map yields a better estimate of anomalies due to other causative sources of greater interest.

Filtering – Regional Removal, Decorrugation, and Upward Continuation

The ambient geomagnetic field strength, about 54,000 nT in our area, dominates the scalar value of total magnetic field intensity and is very consistent across most surveys of archaeological scale. Typically one removes the regional component by a scalar subtraction of the mean value of the acquired observations or by fitting and subsequently subtracting a low order polynomial surface fit to the data. We removed the regional field from our data by subtracting a least squares best-fit plane that decreases about 0.8 nT per meter to the northeast.

Decorrugating by Urquhart's (1988) method involves three general steps. The first step uses a low pass frequency filter to separate the grid of data into its short and long wavelength components in the acquisition direction. Next, the resulting long wavelength component of the grid is long-wavelength filtered (again with a low pass frequency filter) in the direction perpendicular to the acquisition direction. It is this direction, perpendicular to acquisition, which contains short wavelength components resulting from variable heights and nonlinear positioning of the sensor during acquisition of the magnetic observations. The low pass filter removes the short wavelength

components perpendicular to the acquisition direction; these short wavelength components result in corrugations observed in the contoured data. This second step yields a smooth long wavelength grid. Finally, add the smooth long wavelength grid to the short wavelength components isolated in the first step. The result is decorrugated (figure 4). We used Phillips (1997, 2007) implementations for decorrugating and much of the subsequent filtering.

Iterative experimentation is necessary when separating the grids into short and long wavelength components for decorrugation. The best choice of filter wavelengths is determined by examining successive filtering experiments with increasing wavelengths. If one chooses a long wavelength filter that is too long, then images of the noise will contain too much archaeological or geological information. Examining the decorrugated results allows visual confirmation that you are removing the correct wavelengths. Ultimately, this is subjective image processing and the greater the spectral overlap of signal and noise, the more difficult the decision. We used filter lengths of nine samples and nine lines along and across acquisition lines respectively. Representative subgrids from our total magnetic intensity grid show the positive effects of regional removal and decorrugation along with an example of the aliasing parallel to the acquisition direction which we removed (figure 4).

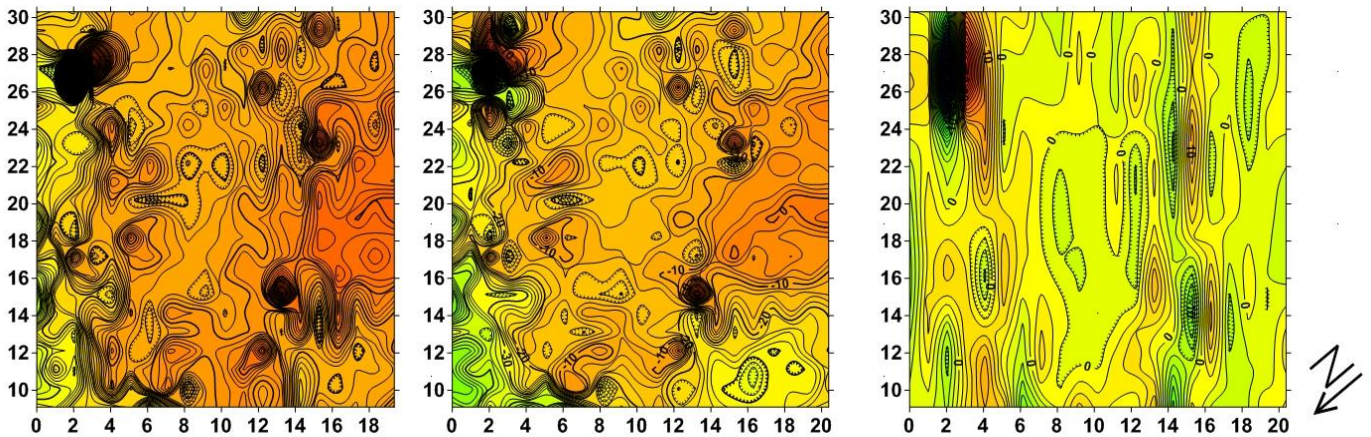


Figure 4. The left image is representative of the total magnetic intensity map with data acquisition parallel to the vertical axis. The central image has had the regional removed and is decorrugated. The right hand image is the corrugation removed from the left

Separating Magnetic Effects of Surface Debris

The left hand edge of our magnetic data (figure 3) parallels a road and an older railroad right of way. Over the years, both were sources of ferromagnetic debris which adds to that left by Cinnabar residents and their farming and ranching operations. This surface scatter is particularly prevalent near the road and yields numerous high amplitude and high gradient magnetic anomalies. Thus, we extracted a subset (Figure 5) from our decorrugated data to demonstrate the utility of matched filtering for separating the magnetic effects of surface debris.

The numerous small dipolar features on the decorrugated magnetic map (figure 5) at the scale of 0.5 to 2 meters result from randomly scattered ferrous sources on or near the ground surface. At the Cinnabar site, these objects include horseshoes, bits of cast iron stoves, scrap sheet metal,

nails, and the like. Such objects have a combination of induced and remanent (permanent) magnetizations. An induced magnetization would typically cause a dipolar signature which is a

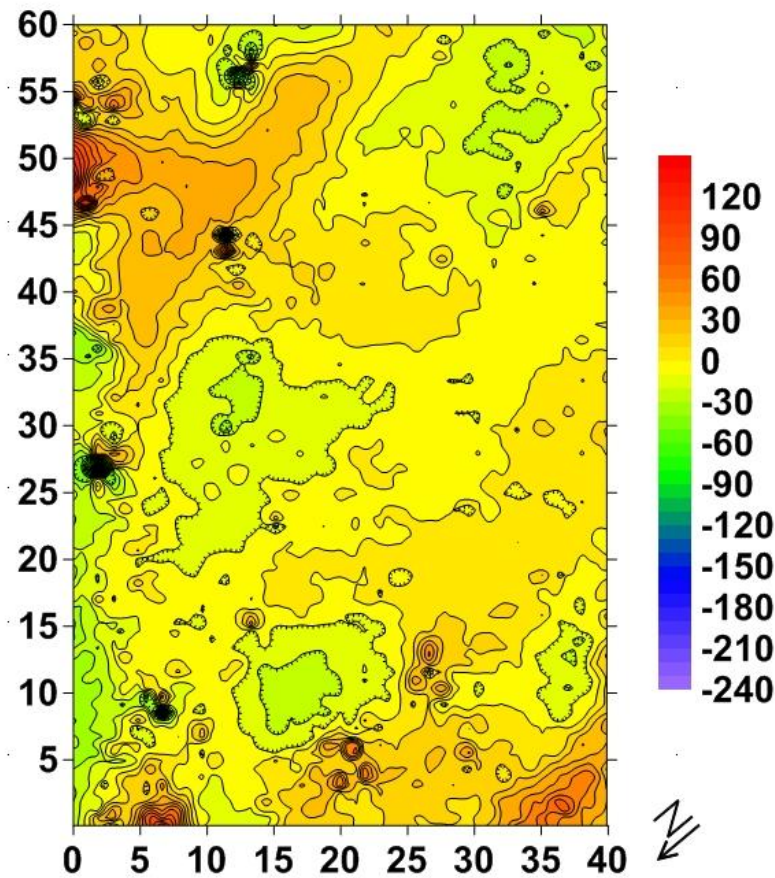


Figure 5. Subset of data highlighting high gradient anomalies at the left edge of the study. Decorrugated total field intensity with planar regional field of about 54,000 nanoteslas removed. The contour interval is 5 nT; horizontal dimensions are meters.

paired set of high and low amplitudes with the low amplitude offset towards magnetic north (12.5° east at the study location). If there is a remanent magnetization vector added to the induced magnetization, the dipole signature points in an alternative direction depending on the vector sum of the induced and remanent magnetizations. These differences in direction are not important in the separation of anomalies by matched filtering.

Finally there are some longer wavelength (~ 10 meter east-west) signals which trend north-south through the area. These features correlate with subtle drainages apparent on satellite imagery. Therefore at least some of the anomalies may result from variable concentration of magnetic minerals in old fluvial deposits. Yet, in the final analysis, there is some suggestion that a few may be cultural features. Typically we wish to separate these longer wavelength anomalies and the shorter wavelength dipolar anomalies. We do so using the general assumption that high amplitude steep gradient anomalies have shallow sources and lower amplitude relatively low gradient anomalies result from deeper sources.

Numerous potential field methods (e.g. Blakely, 1995) exist to attenuate or enhance signals of interest in a magnetic data set. Most of those methods make use of the spatial frequency (or wavenumber) domain following a Fourier transformation of the data. For example, evaluating successive upward continuations (e.g. Jacobsen, 1987) of the total field anomaly to a height of around one to two times the survey's line interval will typically remove the dipolar expression of surface debris at archaeological sites. Upward continuation involves multiplying the power spectrum of the total magnetic field by a filter which decreases exponentially in the spatial frequency domain. Unfortunately, this upward continuation also attenuates high spatial frequency (short wavelength) content beneficial to resolving other features. Differencing successive upward continuations approximates the vertical gradient of the field and isolates shallow sources (figure 6). Alternatively, one can enhance the dipolar features by calculating the analytic signal of the

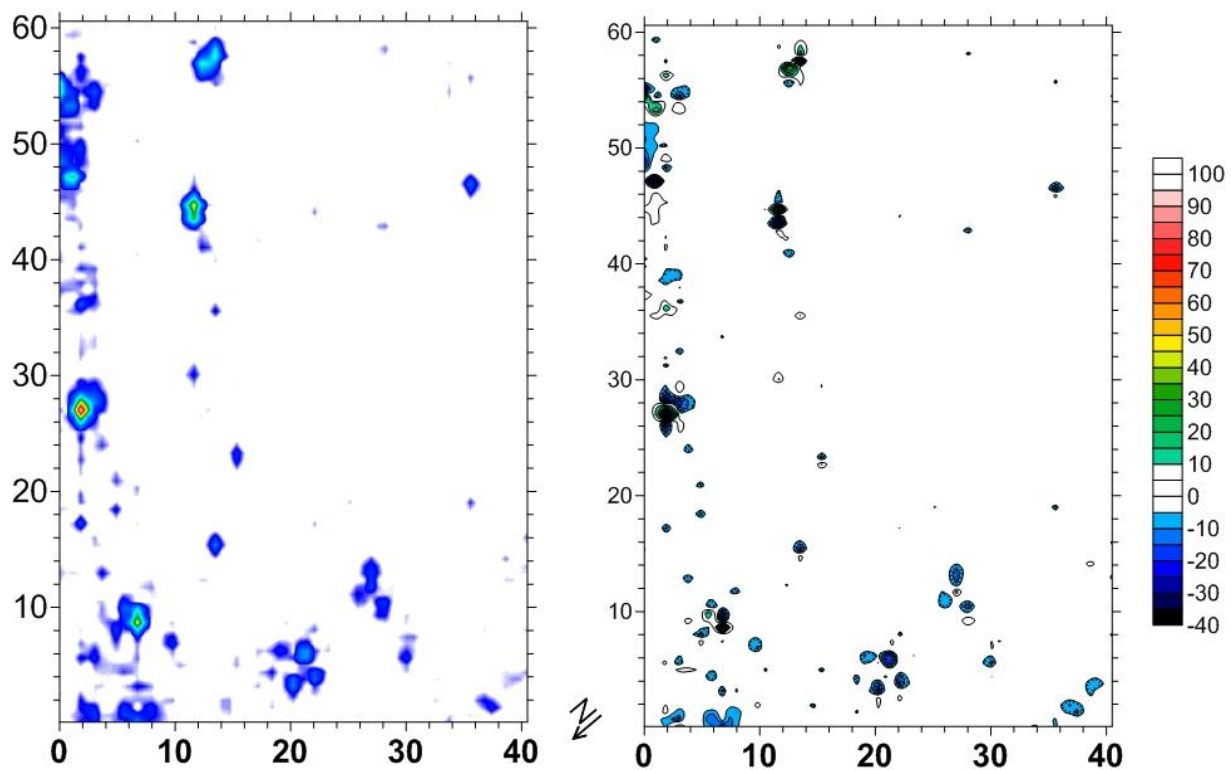


Figure 6. Enhanced signals from causative sources on or near the surface; horizontal dimensions are meters. Left: analytic signal of the total magnetic intensity. Right: synthetic vertical gradient calculated by differencing the total field intensity with an upward continuation of 0.2 meters; the zero contours are suppressed for clarity.

total field (Roest et al., 1992). If one is searching for the sources of those dipolar anomalies missed in a surface survey publicly available Magpick© software by Tchernychev (2008) allows one to interactively pick, locate, and number dipolar anomalies on a magnetic map. Unfortunately, none of these three techniques (analytic signal, differencing upward continuations, or locating dipolar sources) provides a way to remove their contribution to the total field map. Another technique, threshold filtering, removes components of a signal whose amplitudes are below a specified level (the threshold) regardless of their position on the wavenumber axis. White ($1/f^0$) noise is flat in the wavenumber domain. Thus, applying successive threshold filters with increasing thresholds to the data allows one to remove increasing amounts of white noise, sometimes bringing out features not otherwise seen. Threshold filtering decrements signal at a

constant level across the spatial frequency spectrum but the dipolar anomalies typically have high power due to their shallow depth. Therefore the dipolar anomalies are not effectively isolated with threshold filters. Removing components across the frequency spectrum also lowers resolution in edge detection of larger scale features.

Matched bandpass filtering is an effective way to separate magnetic anomalies from different depths. The method is based on equivalent sources (Pedersen, 1991) which are fictional layers below the observation surface where the distribution of magnetization produces the observed magnetic field. Spector and Grant (1970) showed that equivalent source layers at different depths yield radially averaged logarithmic power spectra, from gridded magnetic data, with segments of constant slope. These linear segments in the power spectrum represent magnetic sources at similar depths and characterize features at the principal depth ranges of causative sources. Syberg (1972) proposed matching bandpass filters, in the spatial frequency domain, to the characteristic parts of the power spectrum for different features. Filtering the total field magnetic data with the matched bandpass filter extracts the frequencies corresponding to these principal depth ranges. For example, the spectrum of a layer of magnetic dipoles is linear at high spatial frequencies but becomes concave down and achieves a maximum at low spatial frequencies. Fitting a line to the high frequency end of that power spectrum and removing that component from the total spectrum separates the dipole layer from the remaining signal.

Employing matched bandpass filtering for anomaly separation has a long history (Nabighian et al., 2005) in the application of aeromagnetic data to tectonics, structure, and resource exploration, but not in archaeology. Anomaly separation by matched bandpass filtering in the spatial frequency domain is successful when the signal (feature) of interest dominates one spectral band of the magnetic field's power spectrum. Generally, there may be a noise layer with low-amplitude high-frequency noise related to acquisition, a layer which corresponds to the surface (or near surface) magnetic sources, and one or more additional layers from deeper magnetic sources. In an archaeological study these may correspond to acquisition and instrument noise, debris on or near the surface, somewhat deeper sources such as foundations or compact living surfaces, and possibly a deeper signal from underlying geological sources. Shallow and deeper magnetic sources dominate the high and low spatial frequency ends of the power spectrum respectively.

Matched Filtering of the Example Data

The general idea in matched filtering is to fit the radially averaged power spectrum of the total field magnetic data (figure 3) with a series of power spectra corresponding to simple, equivalent layers at the archaeological site. One then uses the equivalent layer information to construct bandpass filters which separate the original magnetic field data into wavelength groups that contain the magnetic anomalies in each equivalent layer. As noted by Spector and Grant (1970) and later workers, the power spectra of these equivalent layers are linear segments in the log power spectrum of the data. Existing software (Phillips, 1997; Phillips, 2007) based on the contributions of Syberg (1972) facilitates the calculations.

For an example, consider a two layer case consisting of a magnetic dipole layer with amplitude spectra A_1 and average depth d_1 overlaying a deeper magnetic half space at depth d_2 with amplitude spectra A_2 . The depth terms will dominate the spectrum and, ignoring any noise, the total magnetic intensity (TMI), which is their sum, will have two independent linear segments in

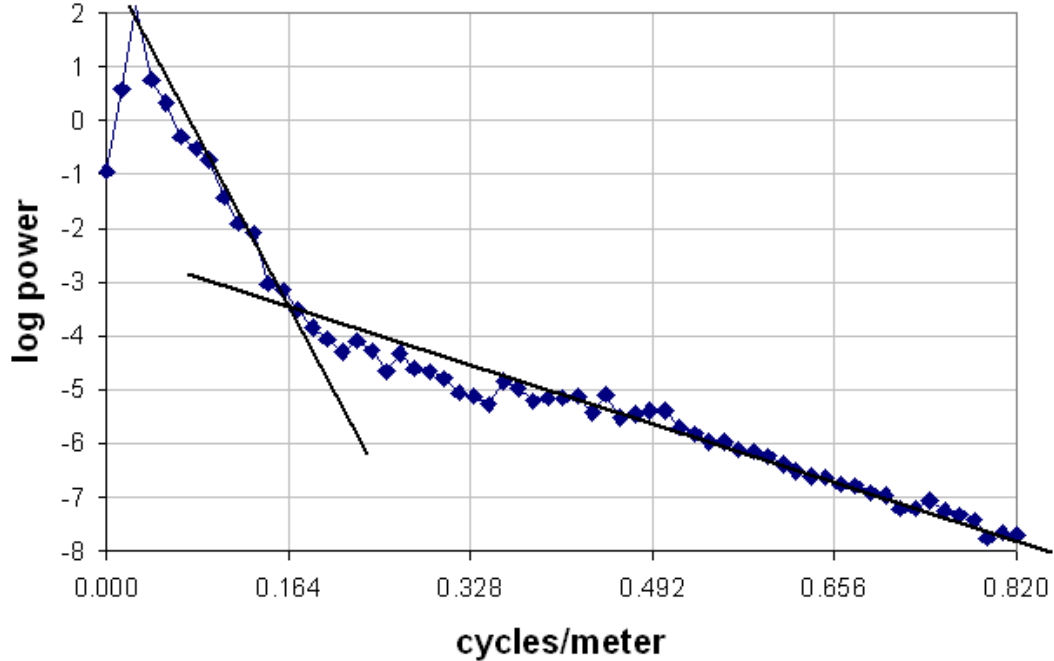


Figure 7. Radially averaged power spectrum of the total magnetic intensity. The symbols show the power spectrum, the solid lines illustrate the separation of two equivalent layers forming the basis for matched bandpass filters as discussed in the text.

its radially averaged log power spectrum. Let their intercepts, at wavenumber (k) = 0, have values of c_1 and c_2 for the dipole layer and deeper half space, respectively. Then, the amplitude spectra for the components look like:

$$A_1(k) = c_1 \exp(-d_1 k)$$

$$A_2(k) = c_2 \exp(-d_2 k).$$

Their combined power spectrum is:

$$E(k) = [A_1(k) + A_2(k)]^2, \text{ or}$$

$$E(k) = [A_1(k) * (1 + A_2(k)/A_1(k))]^2.$$

Substituting for $A_1(k)$ and $A_2(k)$,

$$E(k) = [c_1 \exp(-d_1 k) * (1 + (c_2/c_1) \exp((d_1-d_2)k))]^2.$$

The inverse of the second factor in the previous expression is

$$F(k) = 1 / (1 + (c_2/c_1) \exp((d_1-d_2)k)).$$

$F(k)$ is the filter to separate the shallow magnetic dipole layer from the deeper magnetic half space. Multiplying the Fourier transform of the total magnetic intensity by the filter and then applying the inverse Fourier transform to the product separates the components. The constants c_1 and c_2 are the intercepts of the appropriate linear segments read off the graph of log radial power spectrum versus wavenumber at $k=0$. We obtain the depths d_1 and d_2 from the slopes of the linear segments with depth = $-\text{slope}/4*\pi$ when the horizontal axis is cycles/wavelength. Phillips' (2007) implementation, as used in this study, utilizes a nonlinear least squares refinement to the initial observational fits of linear segments on the log power spectrum.

The radially averaged log power spectrum of our example data has two obvious linear segments (figure 7). The segment with steeper slope at longer wavelengths (fewer cycles per meter) results from relatively deeper sources. The segment with lower slope at shorter wavelengths (more cycles per meter) is from the scattered debris on or near the surface. We calculate the matched bandpass filters (figure 8) for separating equivalent layers as the quotient of the spectrum of each single

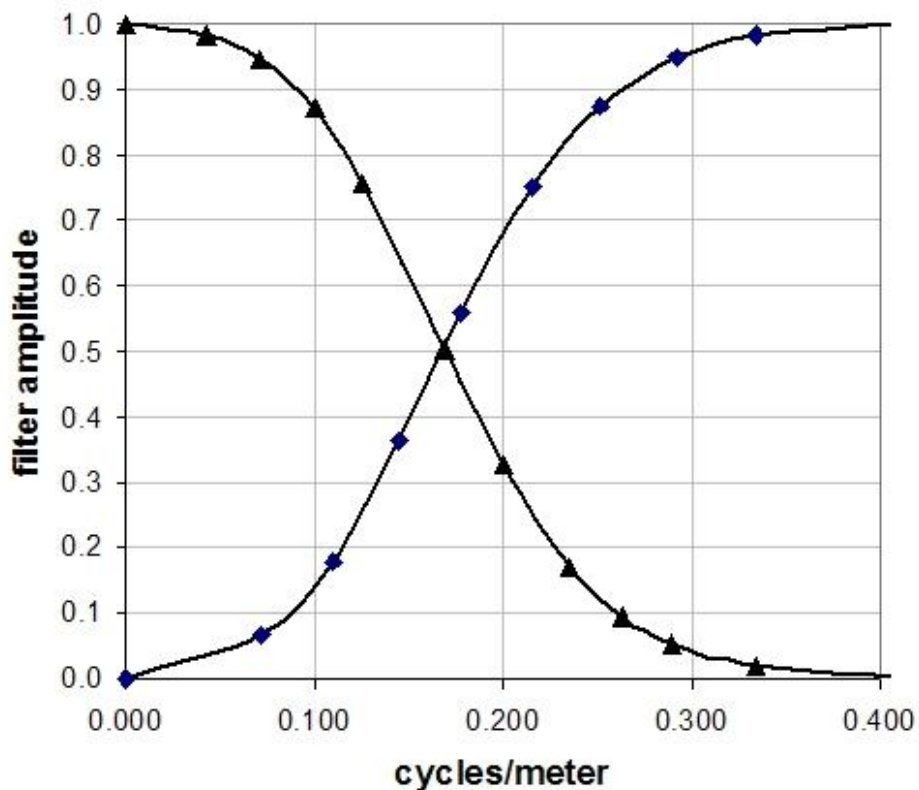


Figure 8. Matched bandpass filters in the spatial frequency domain. Triangles show bandpass for long wavelength signal, diamonds indicate bandpass for short wavelength signals. Parameters for the filters are determined empirically as discussed in the text.

layer divided by the spectrum of the total field (Syberg, 1972). Applying the matched bandpass filters (figure 8) to the Fourier transform of the total field magnetic intensity data (figure 7) separates the magnetic anomalies by their apparent depth to causative sources (figure 9). In this case the equivalent layer for the shallow sources is at 0.5 meters, and that for the deeper sources at 3.0 meters. Those depths indicate adequate separation, but it is worth recalling that there is no inherent depth information in magnetic observations. Adding the two grids (shallow and deep)

would yield the original data set. The benefit of this approach is that the source layers are isolated without losing information as is the case with enhancing surface features using magnetic gradiometry, analysis by upward continuation, or the analytic signal.

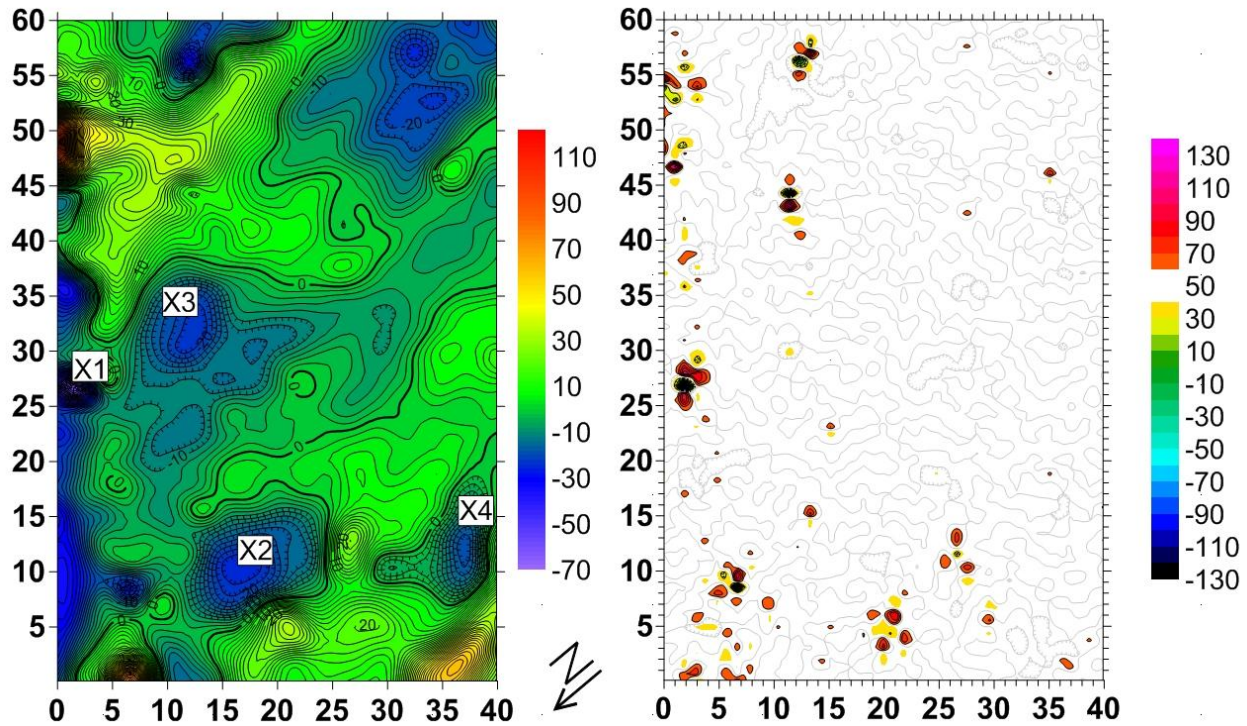


Figure 9. Total field magnetic intensity separated into two equivalent layers; horizontal dimensions are meters. **Left:** magnetic field from the deeper equivalent layer separated by applying the long wavelength bandpass filter to total field intensity; contoured at 2 nT. **Right:** anomalies from on or near surface sources contoured at 10 nT; the zero contour is removed for clarity. The sum of these two maps equals the original decorrugated data (figure 5); X1 through X4 mark locations mentioned in text.

The shallow source components of the magnetic data (figure 9) are well separated from the total field data and obviously distinct from the deeper sources (figure 9). The shallow sources are more concentrated to the left (northeast) of the map, which parallels the long-lived road through the study area. Most of the shallow sources lie on the ground surface and are more reasonably found by visual inspection than by magnetometry. The map of shallow sources bears strong resemblance to the analytic signal of the total field intensity and the synthetic vertical magnetic gradient created by differencing upward continuations (figure 6). Any of these three methods serves to isolate and locate the shallow causative sources. The advantage of separating the shallow sources with matched bandpass filtering is that no information is lost; the remainder of the information remains in the map of deeper sources (figure 9).

Following separation, the magnetic signals from the randomly distributed sources littered on and near the ground surface cause much less degradation of the deeper sourced anomalies (figure 9). There is some spectral overlap in the signals and the filters (figure 8) and areas with apparently larger concentrations of surface debris still have some expression on the map of deeper sources (e.g. X1 labeled on figure 9) but the deeper source layer is now easier to interpret. In particular, magnetic lows labeled X2, X3, X4 (figure 9) have edges, as judged by high magnetic gradients, at

distinct angles to the dominate north-south trend of the underlying fluvial sediments. These three anomalies are strong candidates for future archaeological excavations.

Edge Detection on Isolated Anomalies

Two larger areas of very high amplitude anomalies dominate the right hand edge of our total field intensity data (figure 3). This complicates the separation of sources. The high frequency character of these anomalies demonstrates that the sources are near surface. Because there is not nearly as much contamination from surface debris in this portion of the study area we proceed directly from the decorrugated map to further analysis. Thus, following decorrugation we further attenuated high frequency noise by upward continuing the data by half a meter (one half of our line spacing during acquisition) using standard Fast Fourier Transform (FFT) techniques for level-to-level continuation (e.g. Blakely, 1995). Before calculating the forward FFT for this and subsequent filtering steps we extended the grid by 20% and cosine tapered the result to reduce edge effects and aliasing. Upward continuation mathematically transforms the data measured on one surface to the magnetic field values that would be measured on another surface farther from causative sources. The shorter the wavelength (higher spatial frequency) of the upward continued anomaly, the greater the attenuation. Typically, upward continuation by an amount equal to or less than line spacing attenuates short wavelength noise due to variable motion of the sensor and sources on the surface without undue loss of signal from more significant causative sources. Upward continuation by half of our line spacing produced distinct, characteristic anomalies (figure 10). These anomalies (figure 10) as enhanced by regional removal, decorrugation, and upward continuation are similar to our expectations for anomalies caused by deeper sources such as foundations with spatial dimensions of several meters. That is, the overall anomalies are similar in scale to a building's footprint (e.g., Larson et al., 1999) while magnetic anomalies from individual foundation walls broaden as the depth to their tops increases. In our analysis, we focus on those anomalies because they are of the appropriate spatial scale of interest for our investigation.

Edge Detection on Isolated Anomalies

On inspection of our processed data, we isolated two higher amplitude anomalies (figure 11) with length scales greater than four meters that dominate the contour scale of our total field intensity data. Each anomaly is within our scale of interest for discovering and delineating structures at the periphery of the Cinnabar site. One was the site of preliminary excavation before the magnetic survey. However, the second showed no readily discernible ground evidence of a historic structure and is beyond the area where a historic photograph showed the limits of the town. We extracted the two high amplitude anomalies from the total data set after removing the ambient field, decorrugating, and upward continuing as discussed above.

Given good residual magnetic maps, isolating a target anomaly is a straightforward procedure. For features the size of foundations or compacted living surfaces applying edge detection techniques to the resulting anomalies helps guide the location of initial excavations. A number of edge detection techniques beyond traditional maps of first and second vertical derivatives exist (e.g. Roest et al., 1992; Blakely and Simpson, 1986; Thurston and Smith, 1997; Fedi and Florio, 2001;

Cooper and Cowan, 2008) and several are implemented by Phillips (1997, 2007). As one would

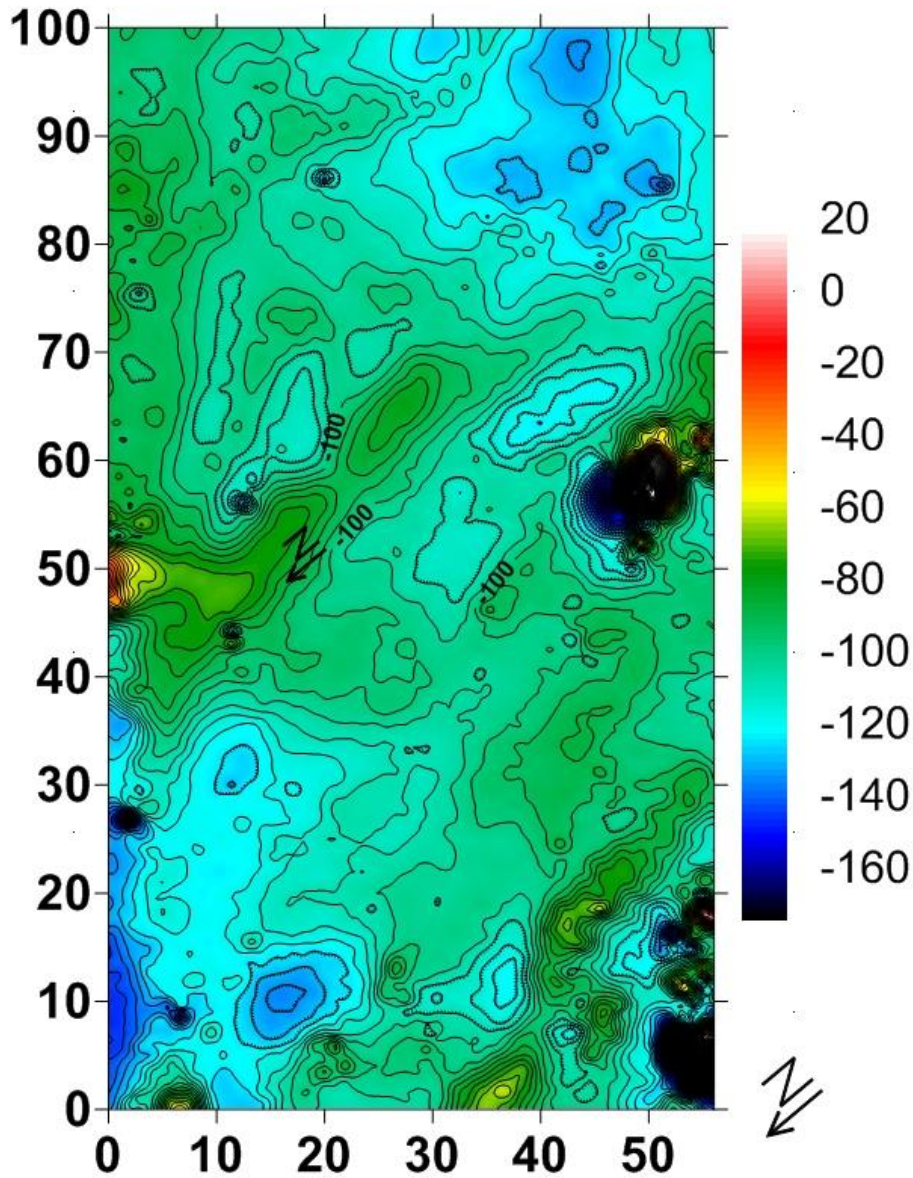


Figure 10. Field intensity contoured at 5 nT following regional removal, decorrugation, and upward continuation of 0.5 meters; total range is 653 nT.

expect, the more that such methods depend on higher order derivatives the more susceptible they are to noise in the data set. Despite decorrugation and upward continuation of the data set, our observations from a historic town site with significant debris on the surface still contain short wavelength anomalies associated with that debris. Thus to delineate edges on the isolated anomalies (figure 11) we use the horizontal gradient method (HGM) of Blakely and Simpson (1986) which only requires first-order derivatives. The value calculated in HGM analysis is the square root of the sum of the squared derivatives of the field in the x and y coordinate directions.

The horizontal gradient method requires that one first subject the magnetic data to one of two different but related transformations. Reduction to pole (RTP) is an FFT-based transformation (e.g., Blakely, 1995) that yields a phase shifted anomaly as if the causative source is located at the

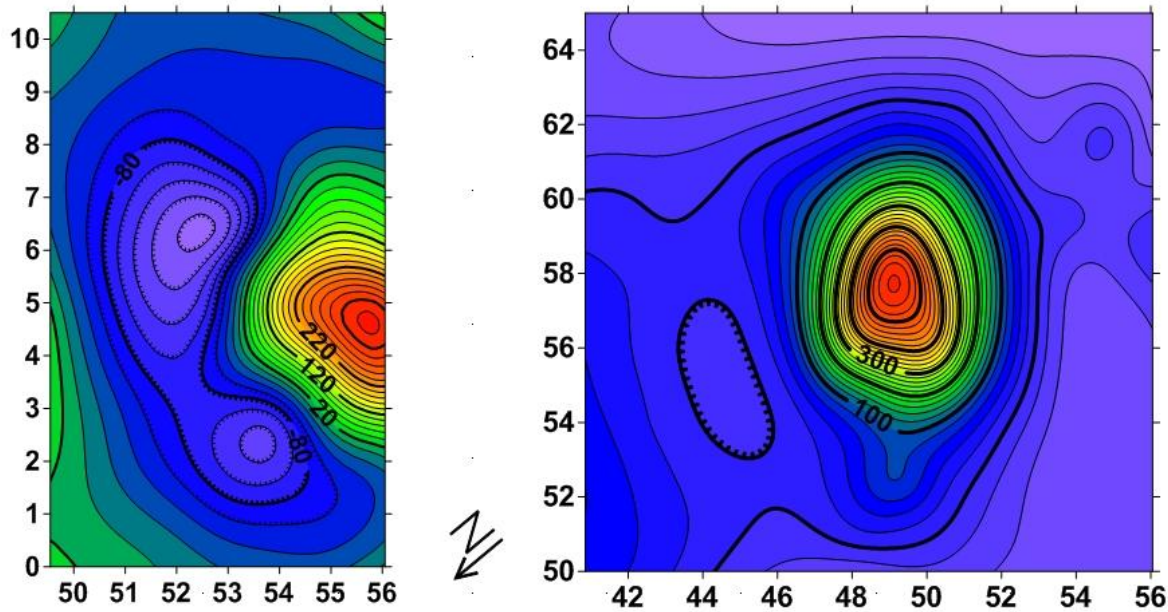


Figure 11, Two anomalies isolated for further interpretation. Each is decorrugated and upward continued by 0.5 meters. Contour interval is 20 nT.

magnetic pole, thereby removing most of the dipolar character of the signal. Poisson's relation shows that for a body with both uniform magnetic susceptibility and density the magnetic potential is proportional to the derivative of the gravity potential in the direction of magnetization. Baranov (1957) exploited this relation to develop the pseudogravity transformation, another linear filter typically applied in the Fourier domain. The pseudogravity transformation yields magnetic scalar potential with vertical magnetization, hence 'pseudogravity' in that the transformed field looks more like a gravity anomaly, centered over the source, which was among Baranov's (1957) intentions. The pseudogravity transformation also accentuates long wavelengths while attenuating shorter wavelengths. RTP and pseudogravity are related in that the pseudogravity is the first vertical integral of the reduction to pole transform (e.g., Phillips et al., 2007). The dependence on RTP transformation presents problems in areas of low latitude with shallow magnetic inclination which is not the case at Yellowstone National Park. For our transformations, we assumed induced magnetization of the soil and sediment was much greater than any remanent magnetization and used the local declination and inclination of 12.5° east, 70° down, respectively.

Typical applications for which HGM was developed have depth scales of kilometers. In that situation, the determination of the appropriate transformation (RTP or pseudogravity) drives the ability to get depth estimates from the method depending on whether the expected source consists of thin or thick sheets. When used solely for edge detection, HGM on a pseudogravity transformation tends to have fewer false contacts than when calculated for an RTP transformation that includes more high frequency effects due to the vertical integral relation of pseudogravity to RTP. In practice, comparing HGM on the two transformations allows one to see where they overlap.

The top two quartiles of maxima in the horizontal gradient of the pseudogravity superposed on the two extracted anomalies outline the estimates of the edges of subsurface causative sources (figure 12) creating the magnetic anomalies. Thus, the maxima serve to help locate initial excavation units. Maxima shown with larger symbols are more significant. The lower two quartiles of

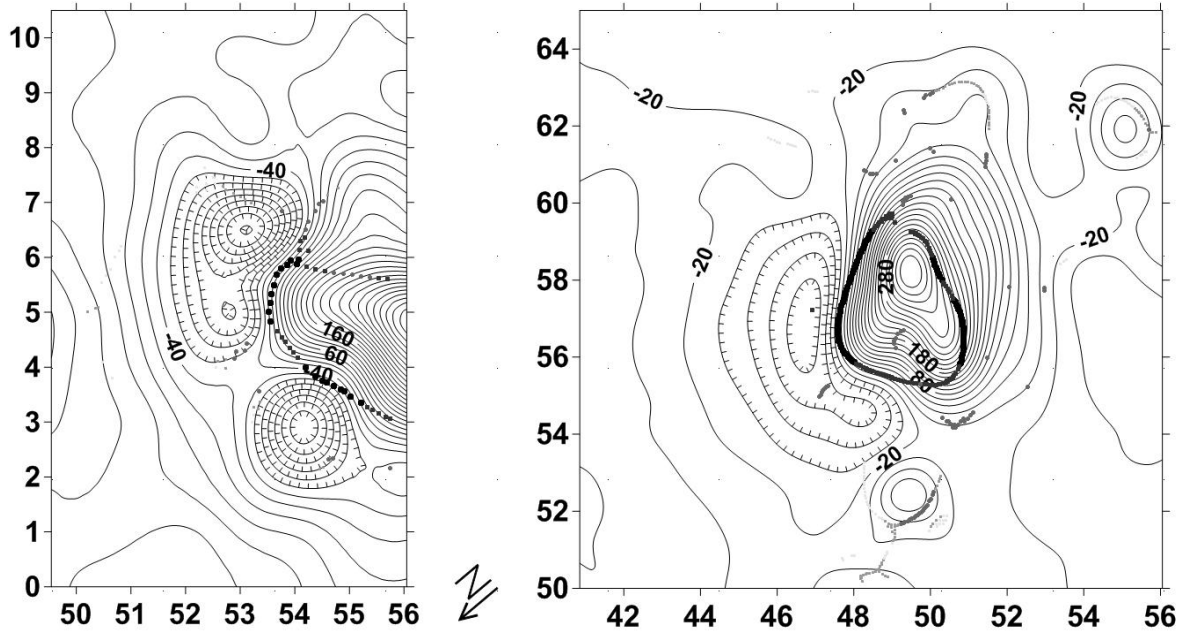


Figure 12. Total field intensity of isolated anomalies contoured at 20 nT. Dots are the superposed maxima of the horizontal gradient of the pseudogravity. Darker and larger dots represent more significant maxima and locate subsurface edges of the causative sources.

maxima (not shown) highlight lesser gradients in the anomalies we judge to be less significant for our interests. These may be from deeper natural sources, remaining noise, or artifacts in the data. For these anomalies, maxima of the horizontal gradient of reduction to pole and pseudogravity transformations were essentially equivalent.

Modeling and Depth Estimates

Magnetic data contain no inherent depth information. Yet, steep gradients on anomalies typically indicate shallow sources and help constrain modeling results which yield a three dimensional model of the subsurface. Another approach to depth estimation uses equivalent sources. Jacobsen (1987) made a strong case for using upward continuation filtering as a method for separating causative sources from various depths. Thus, we experimented with two different approaches to estimating the depth or bottom of the subsurface sources causing the anomalies (figure 12).

First, we inverted the total field data (MAG3D, 2007; Li and Oldenburg, 1996). Those inversions result in best-fit models of subsurface magnetic susceptibility that produce their observed anomalies closely. These three dimensional models thereby provide estimates of depth as well as edges. The plan view (figure 13) and 3D subsurface models (figure 14) generated by MAG3D (2007) compare very well with the maxima of the horizontal gradient of the field intensity results. Thus the two independent methods yield very similar estimates for the edges of the causative

sources. The subsurface magnetic susceptibility models (figure 14) from MAG3D (2007) are three dimensional and thus estimate the depth extent of the sources as well.

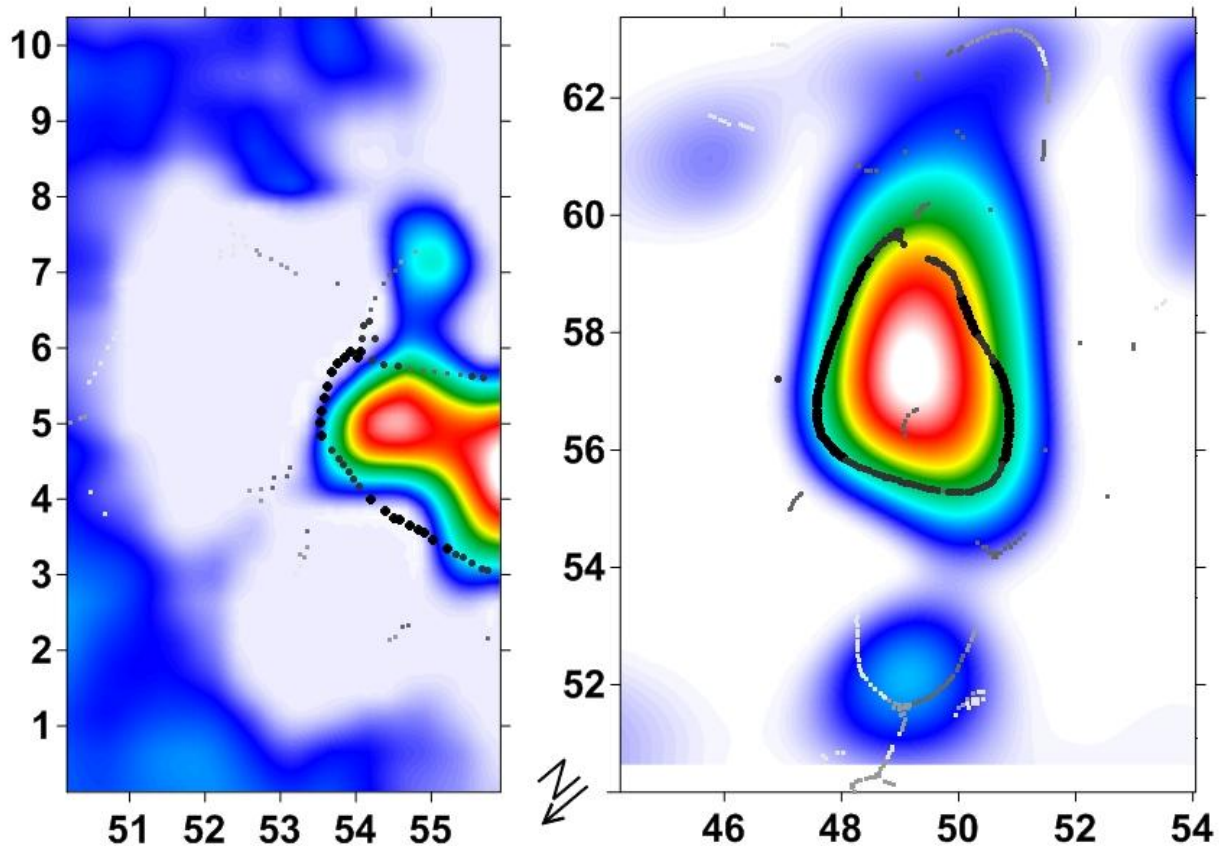


Figure 13. The colored features are the plan view of the causative sources as determined by inverse modeling of the total field anomaly. The shaded dots are maxima of the horizontal gradient; darker and larger dots represent more significant maxima. In both cases, the larger maxima of the horizontal gradient of the field intensity coincide well with the edges of the causative sources as estimated independently by inversion.

We experimented with MAG3D (2007) inversions by generating and constraining solutions a number of different ways, a typical procedure to verify robustness of inverse solutions. For every case, for both anomalies, the depth to the bottom of the causative source was always within about two meters or less of the ground surface. Piro et al. (2007) also successfully used MAG3D (2007) for an archaeological investigation and provide further insights and analysis for its application to other situations. Estimating the depth of sources by differencing successive upward continuations (Jacobsen, 1987) for both of the anomalies suggests that greater than 90% of the equivalent sources are shallower than two meters. Thus, either method indicates sources within the depth range we expect for foundations and further suggest that deeper geologic sources do not generate the anomalies.

Field Testing and Excavations

Subsequent to the magnetic study, we focused archaeological investigations on the two higher amplitude anomalies discussed above to evaluate the possible presence of archaeological features,

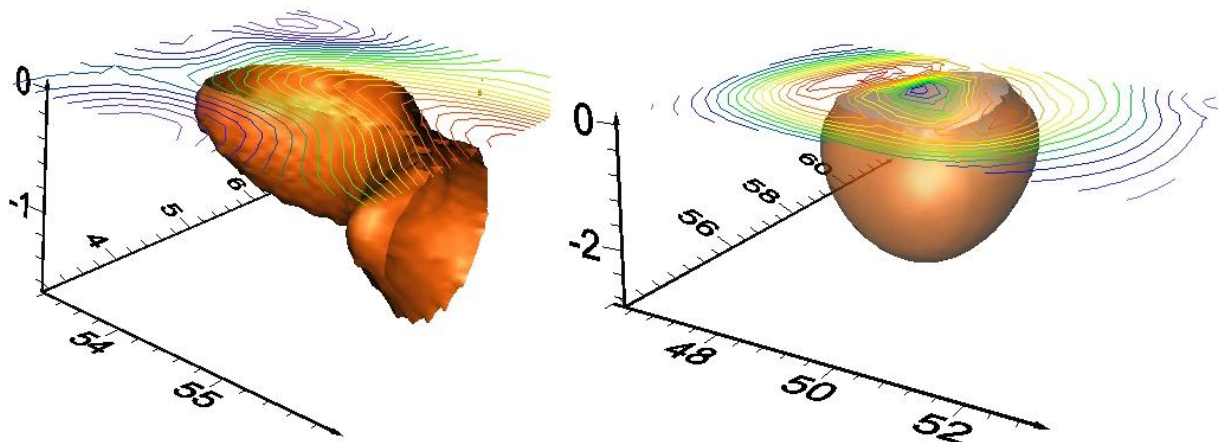


Figure 14. 3D renderings of solutions from the inverse modeling; contours are magnetic field intensity. The depicted isosurfaces are those near the maximum gradient of susceptibility in the inverse solutions.

such as building foundations, buried below the ground surface. Ultimately, we chose to investigate one with an excavation test unit. First we evaluated the area of both isolated anomalies with an in-depth surface reconnaissance.

The anomaly near ($x = 55$, $y = 5$) coincides with a linear surface feature which extends away from Cinnabar to the southeast. We interpret that linear feature to be a former field-access road or irrigation ditch, both of which are common to the project area due to the use of the area for agriculture in the early-mid 20th century (prior to its purchase by Yellowstone National Park). Based on its association with the linear feature, we chose not to subject it to archaeological investigation thinking it has a lower potential for associated archaeological materials. However, based on our positive results from the second anomaly, there are probably remains of a buried historical structure along that old road or irrigation canal.

The area around the anomaly at ($x = 50$, $y = 57$) contained a scatter of historic glass and metal fragments on the ground surface, a possible indication of historic activity associated with Cinnabar. Thus, we excavated two one meter square test units (TU) to investigate the strong magnetic signature of the area. TU 13 is within the central portion of the magnetic anomaly, while TU 14 is approximately 20 meters to the west-northwest (figure 2) outside the area of the larger anomalies (Figure 3). TU14 yielded limited artifacts including a few square nails, a cartridge, a button, and a suspender clip distributed within a few centimeters of the surface, perhaps indicating a house in the area.

Results of archaeological investigations in TU 13, within the magnetic anomaly, documented the presence of an intact archaeological feature within the area, likely associated with a former domestic structure on the southeastern flanks of Cinnabar. Of particular interest, TU 13 yielded a buried living floor containing burned wood fragments, charcoal, mortar, glass, and nails

approximately 15-20 cm below ground surface (figure 15). These artifacts indicate that a structure was present at one time, but possibly burned after or during the abandonment of Cinnabar in the

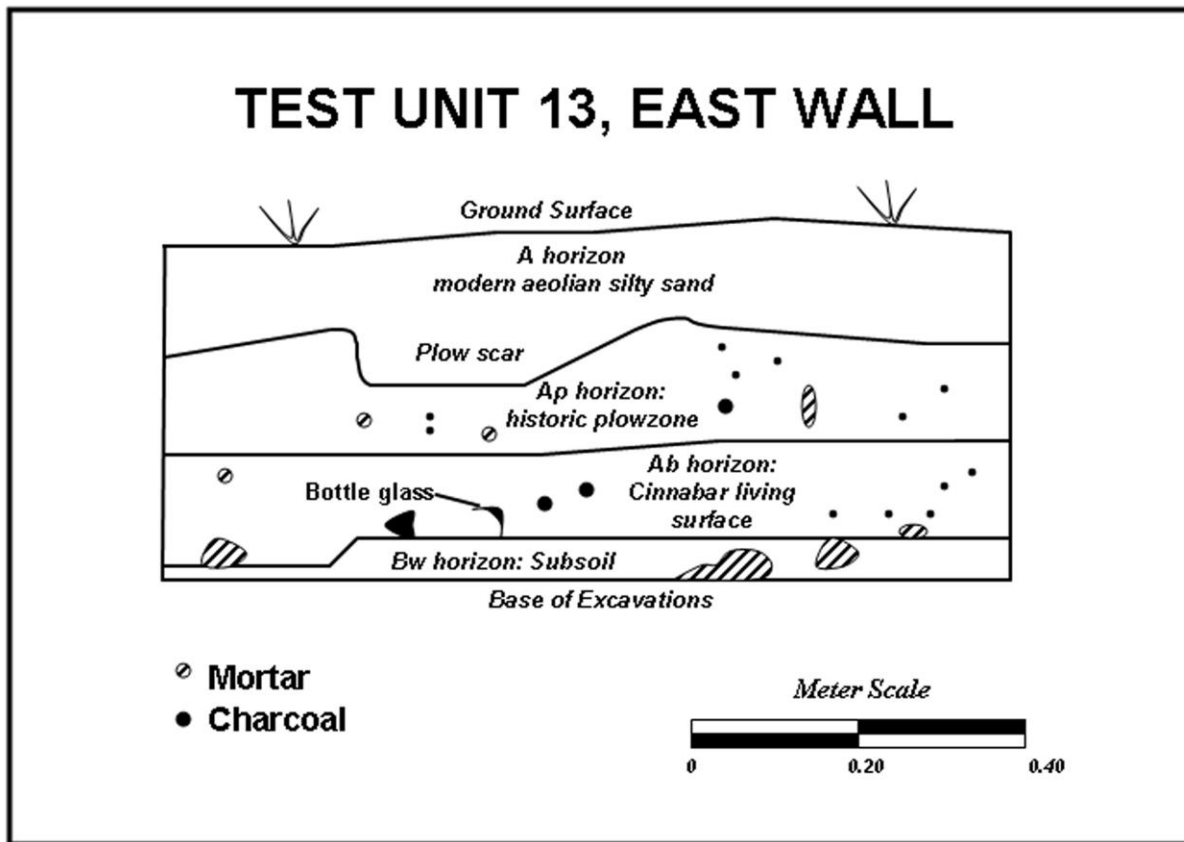


Figure 15. Profile of the east wall from a square meter excavation (Test Unit 13) on the south central anomaly at about x=50 m, y=57 m.

early 20th century. Excavation of TU 13 also identified plow scars stratigraphically above the building remains, suggesting that the area was plowed in the early-mid 20th century, further obscuring the presence of the former building. Finally, after agricultural use of the area ceased in the mid-1900s, a 10-cm thick layer of silty aeolian sand blew over the surface of the feature, effectively masking its presence from the ground surface but not from magnetic detection.

Summary

One component of the Montana-Yellowstone Archaeological Project, a joint endeavor of The University of Montana Department of Anthropology and Yellowstone National Park, was determining the spatial extent of a historic town site, Cinnabar, Montana at the edge of Yellowstone National Park, USA. To help constrain the spatial extent of Cinnabar, we acquired total field magnetic intensity observations over a portion of the proposed southeast extent of the town. We then subjected those observations to various filtering techniques, edge detection, and modeling techniques common in aeromagnetic and ground magnetic exploration for energy and mineral resources.

We processed our data, which were originally quite noisy (figure 3), by first subtracting a slightly dipping ambient field characterized by a first order, best-fit, polynomial surface. Next, we decorrugated the residual field with a two dimensional frequency filter (Urquhart, 1988; Phillips, 2007). Following that decorrugation, we subject two subsets of the data set to different filtering, processing, and interpretational techniques.

For a portion of our data adjacent to a long-lived road and abandoned railroad we use matched filtering to separate the signal from scattered ferromagnetic surface debris from that of deeper archaeological and geological sources. Matched bandpass filtering entails fitting the radially averaged power spectrum of the total field magnetic data with a series of power spectra corresponding to simple equivalent layers at the archaeological site. It is a very effective way to separate magnetic signals from sources on or near the ground surface from signals arising from deeper sources. A major advantage of the technique over magnetic gradiometry, differencing upward continuations, or employing the analytic signal, is we separate the source effects without losing any signal. That is, we are not limited to only collecting signals from the shallowest sources nor do we lose information from deeper sources when we isolate the signal from shallow sources.

A second portion of our data did not have nearly as much signal contamination from scattered surface debris. Following the decorrugation of those data, we used upward continued by one half of the line spacing used during acquisition to reduce acquisition noise. These processing steps successfully isolated the longer wavelength anomalies characteristic of buried foundations or historic building perimeters and greatly reduced the dipolar noise from ferromagnetic objects distributed on the ground surface (figure 3). Once we isolated the anomalies characteristic of foundations, we further accentuated them with standard edge detection and modeling techniques. The horizontal gradient method (HGM) of Blakely and Simpson (1986) provides good estimates of the edges of buried causative sources which coincided well with edges determined by modeling (figure 13). Nabighian et al. (2005) provide the history and complete referencing of these methods and we deem them successful in accentuating features of interest in areas where acquisition is difficult and/or surface scatter contributes significant high frequency noise.

Test unit excavations within the south-central anomaly of this second subset of our data clearly indicate the remains of buried domestic feature, perhaps the foundation to a house or other building associated with the late-19th to early-20th century use of Cinnabar. The lack of surface indicators or adequate historic photography precluded the identification of this buried feature without the aid of the magnetic study. The result is that we identified an important and previously-unidentified domestic feature of Cinnabar through the combined use of total field ground-acquired magnetic data, processing and filtering techniques common in the application of magnetics to energy and mineral exploration, and archaeological excavations. Unfortunately, TU13 was slightly miss-located and did not directly test the edge detection and modeling in that TU13 ended up inside the structure. Ultimately, the collaboration of the two investigative approaches provided important historic archaeological data by which to interpret Cinnabar and its abandonment more than a century ago and contribute to the development of archaeological magnetometry.

References

- Aspinall, A., Gaffney, C., and A. Schmidt, 2008, *Magnetometry for Archaeologists*: AltaMira Press, United Kingdom.
- Baranov, V., 1957. A new method for interpretation of aeromagnetic maps pseudo-gravimetric anomalies. *Geophysics*, 22, 359–383.
- Becker, H., 2001. Duo- and Quadro-sensor Configuration for High-speed/High-resolution Magnetic Prospecting with Cesium Magnetometer. In *Magnetic Prospecting in Archaeological Sites*, H. Becker and J.W.E. Fassbinder, eds. Munich, ICOMOS.
- Blakely, R.J., 1995. *Potential Theory in Gravity and Magnetic Applications*: Cambridge University Press, London.
- Blakely, R. J., and Simpson, R. W., 1986. Approximating edges of source bodies from magnetic or gravity anomalies. *Geophysics* 51, 1494–1498.
- Ciminale, M. and Loddo, M., 2001, Aspects of Magnetic Data Processing. *Archaeological Prospection*, 8, 239-246. DOI: 1-.1002/arp.172
- Cooper, G. R. J., and D. R. Cowan, 2008. Edge enhancement of potential-field data using normalized statistics. *Geophysics*, 73, H1–H4. 10.1190/1.2837309
- Fedi, M. and Florio, G.F., 2001. Detection of potential fields source boundaries by enhanced horizontal derivative method. *Geophysical Prospecting* 49, 40–58.
- Fedi, M. and Florio, G.F., 2003. Decorrugation and removal of directional trends of magnetic fields by the wavelet transform: application to archaeological areas. *Geophysical Prospecting*, 51, 261–272.
- Gaffney, C., Gaffney, V., Cuttler, R. and Yorston, R., 2008. Initial Results using GPS Navigation with the Foerster Magnetometer System at the World Heritage Site of Cyrene, Libya. *Archaeological Prospection* 15, 151-156.
- Jacobsen, B., 1987. A case for upward continuation as a standard separation filter for potential-field maps. *Geophysics*, 52, 1138–1148.
- Kvamme, K.L., 1998. *Geophysical Explorations at the Wuamett Farmstead and the Huyser Farmstead, Minnesota Farmstead Study*. Submitted to BRW, Inc., Minneapolis, MN.
- Larson, T.K., Domers, L.E., Penny, D.M., and Hargrave, M.L., 1999, *Geophysical and Archaeological Investigations of Historic Sites at Fort Riley, Kansas*, US Army Corp of Engineers, Construction Engineering Research Laboratory Technical Report 99/47, 158 p.
- Li, Y., and Oldenburg, D.W., 1996. 3-D inversion of magnetic data. *Geophysics*, 61, 394–408.

MacDonald, D.H., 2007. Final Inventory and Evaluation Report, Yellowstone National Park, Boundary Lands Archaeological Survey & National Register Evaluation, Site 24YE355, Cinnabar/Yellowstone Bank Cache Site. Report submitted to Yellowstone National Park by The University of Montana Department of Anthropology, Missoula, MT.

MAG3D; A Program Library for Forward Modelling and Inversion of Magnetic Data over 3D Structures, version 4.0, 2007. Developed under the consortium research project *Joint/Cooperative Inversion of Geophysical and Geological Data*, UBC-Geophysical Inversion Facility, Department of Earth and Ocean Sciences, University of British Columbia, Vancouver, British Columbia.

Nabighian, M.N., Grauch, V.J.S., Hansen, R.O., LaFehr, T.R., Li, Y., Peirce, J.W., Phillips, J.D., and Ruder, M.E., 2005. The Historical Development of the magnetic Method in Exploration. *Geophysics*, 70, #6, 33-61.

NOAA, 2009, United States National Oceanographic, Atmospheric Administration Space Weather Data and Products. <http://www.swpc.noaa.gov/Data/index.html>; accessed 3/2009.

Odah, H., Abdallatif, T.F., El-Hemaly, I.A., and El-All, E.A., 2005. Gradiometer Survey to Locate the Ancient Remains Distributed to the Northeast of the Zoser Pyramid, Saqqara, Giza, Egypt. *Archaeological Prospection*, 12, 61-68.

Paoletti, V., Fedi, M., Florio, G., and Rapolla, A., 2007. Localized cultural denoising of high-resolution aeromagnetic data, *Geophysical Prospecting*, 55, 421-432.

Pedersen, L.B., 1991, Relations between potential fields and some equivalent sources, *Geophysics*, 56, 961-971.

Phillips, J.D., 1997. Potential-field geophysical software for the PC, version 2.2: U.S. Geological Survey Open-File Report 97-725, 34p.

Phillips, J.D., 2001. Designing matched bandpass and azimuthal filters for the separation of potential-field anomalies by source region and source type: Australian Society of Exploration Geophysicists, 15th Geophysical Conference and Exhibition, Expanded Abstracts CD-ROM, 4p.

Phillips, J.D., 2007. Geosoft eXecutables (GX's) developed by the U.S. Geological Survey, version 2.0, with notes on GX development from Fortran code: U.S. Geological Survey Open-File Report 2007-1355.

Phillips, J.D., Hansen, R.O., and Blakely, R.J., 2007. The use of curvature in potential-field interpretation, *Exploration Geophysics*, 38, 111-119.

Piro, S., Sambuelli, L., Godio, A., and R. Taormina, 2007. Beyond image analysis in processing archaeomagnetic geophysical data: case studies of chamber tombs with dromos, *Near Surface Geophysics* 5, 405-414.

Roest, W. R., Verhoef, J., and Pilkington, M., 1992. Magnetic interpretation using the 3-D analytic signal. *Geophysics* 57, 116–125.

Spector, A., and Grant, F., 1970, Statistical models for interpreting aeromagnetic data: *Geophysics*, 35, 293-3302.

Syberg, F. J. R., 1972. A Fourier method for the regional-residual problem of potential fields. *Geophysical Prospecting*, 20, 47–75.

Tabbagh, J., 2003. Total Field magnetic Prospection: Are Vertical Gradiometers Measurements Preferable to Single Sensor Survey? *Archaeological Prospection*, 10, 75-81. DOI: 10.1002/arp.193

Tchernychev, M., 2008. Magpick, Software for Magnetic processing and interpretation. www.geometrics.com.

Thurston, J. B., and Smith, R. S., 1997. Automatic conversion of magnetic data to depth, dip, and susceptibility contrast using the SPI method. *Geophysics* 62, 807–813.

Tsivouraki, B. and Tsokas, G.N., 2007. Wavelet Transform in Denoising Magnetic Archaeological Data. *Archaeological Prospection*, 14, 130-141. DOI: 10.102/arp.289

Urquhart, T., 1988. Decorrugation of enhanced magnetic field maps. 58th Annual International Meeting, SEG, Expanded Abstracts, 371–372.

Acknowledgements

Gradient Geophysics Inc. of Missoula, Montana, distributor of MAG3D, provided use and support of MAG3D for our investigation of its use at the archaeological scale. We thank A. Johnson of Yellowstone National Park and C. Whitacre of the Rocky Mountain Cooperative Ecosystem Unit for funding and logistical support for our archaeological endeavors.